

pubs.acs.org/acscatalysis Research Article

Epoxidation and Late-Stage C—H Functionalization by P450 Taml Are Mediated by Variant Heme-Iron Oxidizing Species

Rosa V. Espinoza, Mark A. Maskeri, Aneta Turlik, Anjanay Nangia, Yogan Khatri, John Montgomery, K. N. Houk, and David H. Sherman*



Cite This: ACS Catal. 2022, 12, 3731-3742



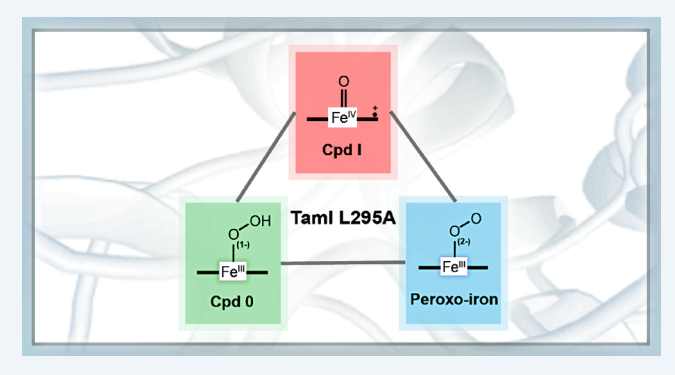
ACCESS I

III Metrics & More

Article Recommendations

s Supporting Information

ABSTRACT: P450-catalyzed hydroxylation reactions are well understood mechanistically including the identity of the active oxidizing species. However, the catalytically active heme-iron species in P450 iterative oxidation cascades that involve mechanistically divergent pathways and distinct carbon atoms within a common substrate remains unexplored. Recently, we reported the enzymatic synthesis of trifunctionalized tirandamycin O (9) and O' (10) using a bacterial P450 TamI variant and developed mechanistic hypotheses to explore their formation. Here, we report the ability of bacterial P450 TamI L295A to shift between different oxidizing species as it catalyzes the sequential epoxidation, hydroxylation, and radical-catalyzed epoxide-opening cascade to create new tirandamycin antibiotics. We also provide



evidence that the TamI peroxo-iron species could be a viable catalyst to enable nucleophilic epoxide opening in the absence of iron-oxo compound I. Using site-directed mutagenesis, kinetic solvent isotope effects, artificial oxygen surrogates, end-point assays, and density functional theory (DFT) calculations, we provide new insights into the active oxidant species that P450 TamI employs to introduce its unique pattern of oxidative decorations.

KEYWORDS: P450-catalyzed iterative oxidation cascade, P450 TamI, heme iron, epoxidation, hydroxylation, epoxide opening, tirandamycin antibiotics

1. INTRODUCTION AND BACKGROUND

The large superfamily of heme-containing cytochrome P450 enzymes catalyze a myriad of important chemical reactions including, but not limited to, aromatic and aliphatic hydroxylations, epoxidations, ring formation, and C–C bond cleavage. Not only are the P450-catalyzed reactions critical in the degradation of xenobiotic compounds, but they are essential for the biosynthesis of structurally complex bioactive molecules. These versatile monooxygenases can perform precise chemical reactions with high levels of selectivity while overcoming innate substrate reactivity.

When a small-molecule substrate binds to the P450 active site, it displaces the water molecule acting as a sixth ligand of the heme-iron and shifts the enzyme from a low-spin system to a high-spin ferric state (Figure 1; iron species A to B). $^{1,6-8}$ This shift increases the redox potential (100–230 mV) and facilitates the first electron transfer from the redox partners (species C). Molecular oxygen then binds to the iron center, generating the oxy-ferrous intermediate (species D) that can accept a second electron transfer to form the key ferric-peroxo anion intermediate (FeO₂⁻, species E). Subsequent proton transfer (typically supplied by the bulk solvent) to the distal oxygen atom is facilitated by a highly conserved active site

acid—alcohol pair and bound water molecules leading to the ferric hydroperoxide compound 0 (Cpd 0, FeO₂H). A second protonation event facilitates the O–O cleavage step generating the high-valent iron-oxo species compound I (Cpd I, FeO^{IV}), resulting in the release of a water molecule. Found in the oxygen-binding groove of the I-helix, the acid—alcohol pair is thought to be essential for the two sequential protonation events necessary to form Cpd I from the ferric-peroxo species, Cpd 0. However, a few exceptions exist where an alanine or asparagine occur in place of the conserved alcohol residue such as in the case of P450eryF¹² and P450cin, where the substrate harbors a hydroxy functionality that is thought to act as the conserved alcohol residue and asparagine is believed to retain a water molecule, respectively. Moreover, throughout the P450 catalytic cycle, the peroxo states (species D and F)

Received: January 20, 2022



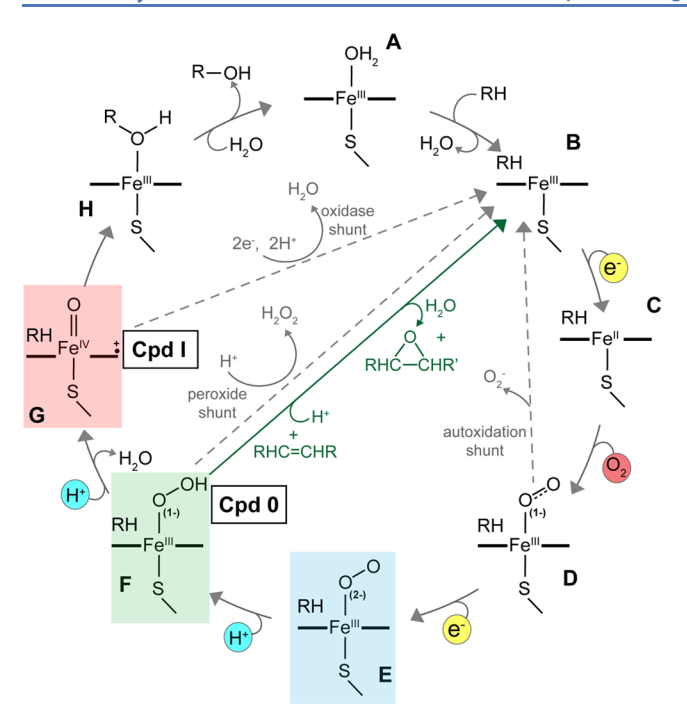


Figure 1. General cycle for cytochrome P450 catalysis. The three unproductive uncoupling pathways are shown with dashed arrows. Alkene epoxidation catalyzed by Cpd 0 species is shown with a green arrow.

can undergo uncoupling and release peroxides while regenerating the ferric form of the enzyme.

Identification of the oxidant species in P450 catalysis remains a central question, and kinetics, substrate atom labeling, spectroscopy, and computational methods can provide key evidence for the different oxygen species driving a mechanistic pathway.⁶ For example, the ferric-peroxo anion

intermediate (Figure 1; species E) can perform a nucleophilic attack on the ketone of the substrate leading to the C-C bond cleavage, as observed in the P450 CYP17A1 involved in human steroid hormone biosynthesis. 14,15 Alternatively, the ferric peroxide species can be protonated to form Cpd 0 (species F), which enables epoxidation via double bond oxygen insertion, as revealed for P450 PimD in pimaricin biosynthesis (where the substrate's topology does not favor catalysis via Cpd I).¹⁶ Alternatively, double protonation leads to the high-spin intermediate Cpd I (species G), the catalytic species considered to be the primary oxidant for most of P450catalyzed oxidations, which include C-H hydroxylation by P450 CYP19A1. 17-19 Relatively little is known about the active oxidizing species in iterative oxidation cascades involving mechanistically distinct pathways and multiple carbon sites within a substrate. The current analysis was driven by the hypothesis that iterative P450 enzymes may shift from one catalytically active heme-iron species to another to modulate their stepwise sequence with exquisite selectivity on a common substrate. Elucidating the oxidant species involved in P450based multistep biocatalytic systems may inspire the engineering of homologous enzymes to expand the range of oxidation reaction types for catalyst-controlled, cascade reactivity.

The *Streptomyces*-derived P450 TamI is an iterative enzyme responsible for the late-stage oxidation of tirandamycin C (1) to B (5), the terminal product of the tirandamycin biosynthetic pathway and the most potent congener in bioactivity against an array of human pathogens including vancomycin-resistant *Enterococci faecalis* (Figure 2). As a result of intrinsic substrate reactivity, TamI performs methylene C10 hydroxylation, C11/12 alkene epoxidation, and C18 methyl hydroxylation in a strict sequence. We recently described the engineering of P450 TamI biocatalysts that alter the iterative process, site selectivity, and number of reactions performed in a catalyst-controlled fashion. This work demonstrated the enzymatic

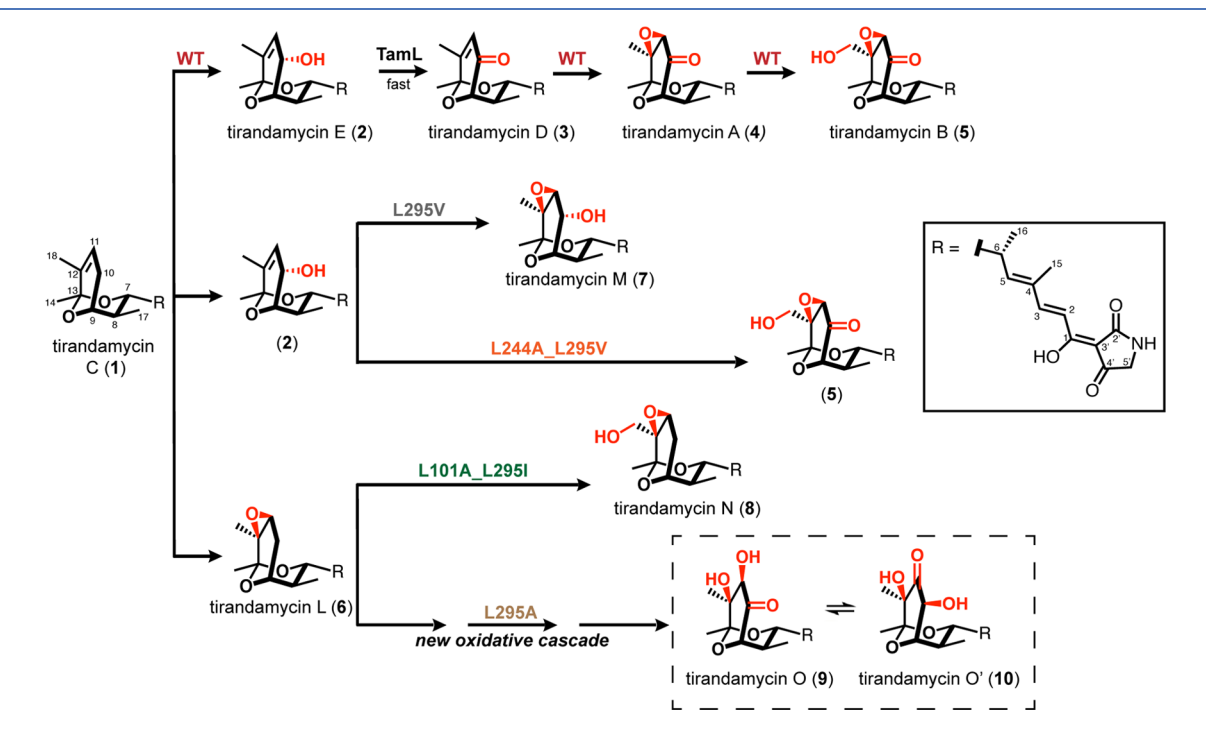


Figure 2. Late-stage iterative oxidative cascades catalyzed by P450 TamI and variants. Naturally occurring tirandamycins include 1–5. New metabolites generated from TamI mutants include 6–10.

Figure 3. Proposed mechanisms for the generation of $1 \to 6 \to 7$ or $7' \to 9$ and 10 catalyzed by P450 TamI L295A. Three mechanisms are described using the nucleophilic peroxo-iron (blue box), Cpd 0 (green box), and Cpd I (red box) as oxidant species.

synthesis of five novel tirandamycin congeners including trioxidized tirandamycin O (9) and O' (10) (Figure 2). The role that variant reactive oxygen species play in mediating the iterative sequence and flexibility of TamI and its mutants for catalyzing mechanistically divergent oxidative reactions has not been previously established. It is this gap in knowledge that motivated the current study, with the expectation that deeper insights may facilitate the rational design for bioinspired catalysis.

Based on the stepwise oxidative sequence exclusively catalyzed by TamI L295A to convert $1 \rightarrow 6 \rightarrow \rightarrow \rightarrow 9$ and 10 (Figure 2) and the unusual oxidation pattern of the trioxidized terminal products, we hypothesized that this P450 variant shifts from one catalytically active oxidant species to another. First, TamI L295A forms 6 by catalyzing a C11/12 double bond epoxidation on 1 rather than a C10-(S) hydroxylation, as observed in WT enzyme, indicating a possible Cpd 0-mediated mechanism. The inherent reactivity of 6 was explored for primary C18 and secondary C10 hydroxylation reactions. 10 Hydroxylation at both positions exhibited similar energetic barriers, suggesting that the formation of either C-H functionalization product is favorable when using 6 as a substrate, with a slight preference for C10 oxidation (0.6 kcal/mol difference). We rationalized that hydroxylating the C10 position on 6 makes the C11 site more electrophilic and prone to opening of the epoxide. As previously established, C10 hydroxylation via Cpd I-mediated catalysis is anticipated.8 Thus, we hypothesized that TamI L295A catalyzes a C10 hydroxylation on 6 to form 7 and/or 7' (the C10 epimer of 7; Figure 3). However, these proposed transient intermediates are not detected in in vitro enzymatic assays when incubating 1 or 6 with the enzyme. 10 This could imply that once 6 is oxidized to 7 or 7', the hydroxy-containing intermediate is not released from the enzyme active site pocket

but is instead instantly oxidized to obtain the final products. Given that congener 7 is available as an authentic standard (obtained from preparative-scale enzymatic reactions), 10 enzymatic reactions with 7 and TamI L295A were performed. Incubating 7 with TamI L295A at increased catalyst loading conditions led to low-level formation of 9 and 10 (Figure S14; lane 14). These results provide compelling evidence that 7 is a transient intermediate toward 9 and 10 under these experimental conditions. The nominal production of the terminal products and the lack of spin shift observed upon the titration of 7 to the enzyme suggest that 7 might not be the preferred transient intermediate in L295A-catalyzed nucleophilic pathways (e.g., Figure 3 blue and green boxes) or that the additional oxidative decorations in 7 impact the substratebinding affinity, making it a poorer fit in TamI L295A active site. Computational analysis showed that 7' exhibits an internal hydrogen bond from the hydroxy to the epoxide, stabilizing its configuration and activating the epoxide for opening (Figure S15). This might suggest that 7' could be a preferred transient intermediate in the L295A-catalyzed pathway; however, this congener is not available as an authentic standard. We suspected that 4 might also be an intermediate in this oxidative cascade; however, no product was observed when incubating 4 with TamI L295A, even at increased catalyst loading. Hence, we postulate that TamI L295A hydroxylates 6 at C10 forming intermediates 7 and/or 7' prior to the oxidative cascade leading to 9 and 10.

After C10 hydroxylation, TamI L295A catalyzes an epoxideopening cascade not previously observed with P450 TamI chemistry. This may indicate the potential involvement of different oxidants en route to 9 and 10. Hence, we proposed three potential mechanisms for the formation of 9 and 10 by TamI L295A including (1) attack by the nucleophilic ferricperoxo to open the epoxide at the C11 site yielding the ketone

(Figure 3; blue box), (2) incorporation of the hydroperoxide Cpd 0 leading to C11 hydroxylation, followed by oxidation to form the α -hydroxy ketone (green box), and (3) H10abstraction by the electrophilic higher-valent metal-oxo species Cpd I generating a free radical that leads to epoxide ring opening (red box). Thus, we sought to explore the identity of the active oxidant species in P450 TamI L295A responsible for catalyzing the iterative oxidation cascade from $1 \rightarrow 6 \rightarrow 7$ or $7' \rightarrow 9$ and 10 and three proposed mechanisms toward the exclusive formation of 9 and 10. In this effort, we (1) disrupted the proton relay network by site-directed mutagenesis that is required for dioxygen activation, (2) assessed the utility of exogenous oxygen surrogates and reactive oxygen species (ROS) scavengers to support P450 TamI catalysis, and (3) calculated kinetic solvent isotope effects (KSIEs) on the steady-state turnover of P450 TamI in its hydroxylation, epoxidation, and unusual oxidative cascade functionalities. Additionally, quantum mechanics (QM) calculations using density functional theory (DFT) were conducted to provide insights into the contribution of the plausible reaction mechanisms and different oxidant species in the P450 catalytic cycle for generating structurally unique metabolites 9 and 10.

2. RESULTS

2.1. Mechanism of Epoxidation via Cpd 0 to Form 6 from 1. 2.1.1. Structure-Derived Mechanism. In P450 TamI, the WT enzyme catalyzes the C10 allylic hydroxylation of 1 to generate 2. The substrate-bound crystal structure of the enzyme revealed that the C10-H (S) σ -bond points toward the heme-iron within a 4 Å distance, prone for hydroxylation to occur via a hydrogen abstraction and rebound mechanism.²⁰ This C-H functionalization reaction likely occurs through involvement of the electrophilic species Cpd I, as previous experimental and theoretical work supports this mechanism for P450-catalyzed hydroxylation reactions.⁸ However, a subtle variation in the active site TamI L295A mutant changed reactivity from C10 hydroxylation to C11/12 epoxidation on substrate 1 to form 6. Previous DFT calculations with 1 revealed that the transition-state (TS) barrier for C11/12 (R/ S) epoxidation is higher in energy (19.2 kcal/mol) than hydroxylation at C10 or C18 sites (14.5 and 16.6 kcal/mol, respectively).²⁰ Thus, we hypothesized that TamI L295A may reorient the substrate to lower the activation barrier and/or favor a different oxidant species to facilitate the energetically disfavored epoxidation reaction over the C-H functionalization product.

Seeking structural confirmation of this hypothesis, we sampled the binding conformations of substrate 1 in Cpd I TamI L295A, utilizing our previously disclosed MD simulations.²⁰ Close examination of the five top occupied clusters of frames suggests that the π -orbitals of the conjugated C11/12 system point away from the iron at a 115.9° angle to the heme (Figure 4).²⁰ While MD simulations are inherently dynamic and these binding conformations may not represent the pre-TS resting conformation, this angle differs from the angles calculated in simulations with TamI WT and 3 and TamI L101A L295I and 1, where diastereoselective C11/12 alkene epoxidation is observed experimentally. In the latter cases, the C11/12 alkene of 3 and 1 points toward the iron at a 90-93° angle to the heme facilitating double bond epoxidation, in agreement with in vitro results (Figure S1). By contrast, in TamI L295A, the geometry of 1 does not favor epoxidation by a synchronous trajectory of oxygen insertion or a charge-

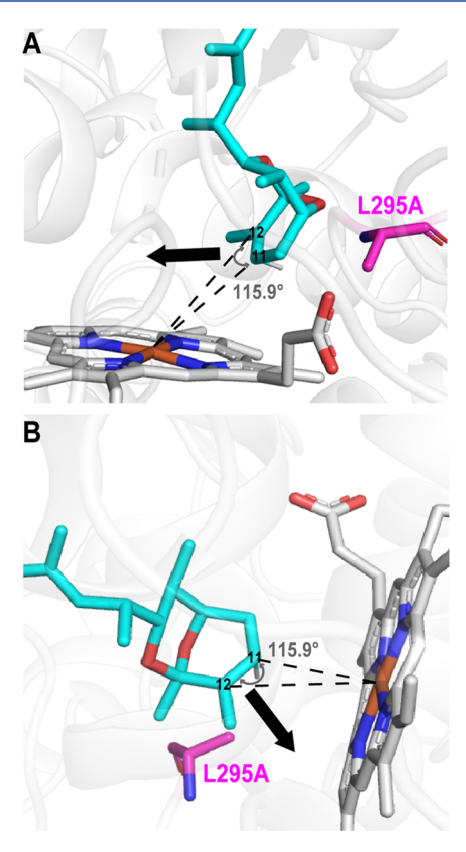


Figure 4. Molecular dynamics (MD) simulations of TamI L295A in complex with **1**. Two different views emphasizing the orientation of the C11/12 alkene are depicted. Black arrows show the orientation of the C11/12 π -orbitals.

transfer complex via a radical or cationic pathway. Instead, the proximity (<4 Å) of the C11-H σ -bond to the heme-iron seems favorable for Cpd I-mediated hydroxylation. However, as noted with P450 PimD and the 4,5-desepoxypimaricin substrate, the energy required to abstract a hydrogen from a vinyl carbon is prohibitive. This led us to hypothesize that the hydroperoxo Cpd 0 species may be the active oxidant in TamI L295A for the first reaction step of its iterative oxidative cascade (Figure 2), where a concerted insertion of the distal oxygen into the C11/12 double bond of 1 occurs to generate 6. The lengthened O–O bond in the hydrogenated peroxide species (Cpd 0) would bring the distal oxygen even closer to the C11/12 π -orbitals of 1, enabling a productive topology of the substrate for C11/12 epoxidation to occur over C10 hydroxylation.

2.1.2. Disrupting the Conserved I-Helix Alcohol Residue for Evidence of Its Role in Catalysis. In P450 TamI, the conserved acid—alcohol pair is composed of Glu251 and Thr252. However, Thr253 resides at the adjacent position that could contribute to the I-helix proton relay network or supplant Thr252 if absent.²³ Mutation of the conserved alcohol residue in P450s is thought to interrupt the second proton transfer, resulting in accumulation of the Cpd 0 species and diminishing substrate oxidation rates while increasing uncoupling of the enzyme and hydrogen peroxide formation. ^{10,11,20,22,23} For example, P450cam catalyzes hydroxylation of its native substrate camphor with high levels of efficiency. However, its variant T252A produces little to no hydroxylated product and instead was found to be capable of performing olefin epoxidation.²² This result was presented as experimental

evidence for the reactivity of a hydroperoxo-ferric Cpd 0 species in the P450cam system.

We created threonine mutants of P450 TamI L295A to probe their role in oxygen activation and catalysis (Figure 5).

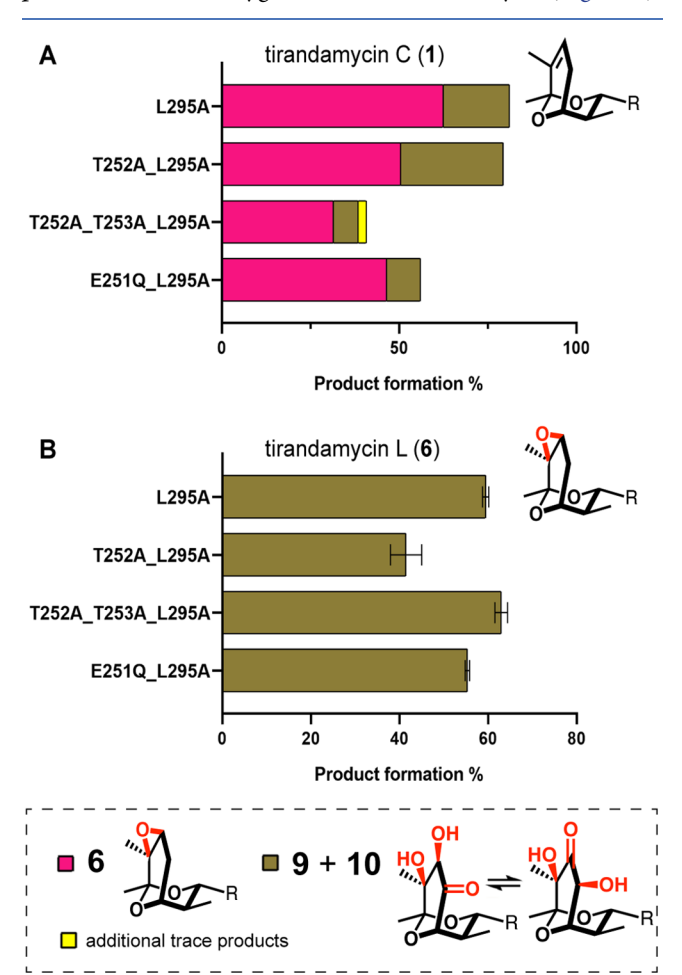


Figure 5. End-point assays with TamI mutants. (A) Reactions with tirandamycin C (1) substrate and (B) reactions with tirandamycin L (6) substrate. Substrates are shown next to each bar graph. Ratios of product formation were estimated based on HPLC traces. The error bars represent the standard deviation of experiments performed in duplicate. For the definition of *R*, see Figure 2. For additional reactions, see Supporting Information.

When incubated with 1, variant T252A_L295A showed a similar product formation to TamI L295A generating a mix of 6, 9, and 10, while triple mutant T252A T253A L295A showed decreased yields. Both threonine mutants displayed reduced hydrogen peroxide formation compared to TamI L295A, suggesting that fewer free radicals occur in these systems (Figure S3). This was further supported by the observation that the TamI L295A-catalyzed oxidation of 1 to 6, 9, and 10 increased in the presence of ROS scavengers (ascorbate, catalase, and dismutase) in a dose-dependent fashion, indicating uncoupled formation of free radicals in TamI L295A (Figures S4–S6). Nonetheless, this increase in product formation could also derive from the fact that these chemical scavengers are able to protect the enzyme, substrate, and/or products from superoxide-induced radical damage. Additionally, the lowered product and hydrogen peroxide formation observed in triple mutant T252A T253A L295A with 1 may indicate that the proton channel to the proximal

and distal oxygen atoms of Cpd 0 has been disrupted in this system. Lastly, the double and triple variants displayed tighter substrate-binding affinity values compared to TamI L295A (Table S1), showing that mutating the threonine residues does not impact substrate binding in an unproductive manner.

The mutagenesis results described above show that altering the conserved alcohol pair in TamI to an alanine (and is thus unable to accept a hydrogen bond from Cpd 0 to drive the O—O cleavage and form Cpd I) does not inhibit catalytic activity. In fact, similar product formation to L295A is observed for C11/12 epoxidation of $\bf 1$ to $\bf 6$ with threonine mutants, suggesting that Cpd 0 may be a viable oxidant for L295A-catalyzed epoxidation.

2.1.3. Investigation of Oxygen Surrogates Supporting Cpd 0 Reactivity. Next, we investigated exogenous oxygen surrogates to assess differences among TamI P450 mechanisms. Hydrogen peroxide can provide the oxygen atom and electrons necessary to overcome the need for molecular oxygen and NADPH-derived reducing equivalents in P450s.²⁴ Therefore, the direct addition of hydrogen peroxide to ferric P450 is expected to form ferric hydroperoxide Cpd 0. However, it is important to note that Cpd 0 can subsequently and irreversibly convert to Cpd I. Therefore, its role in TamI catalysis can only be postulated.

Alternative organic oxidants such as iodosobenzene would not be able to generate Cpd 0 and insert the distal oxygen atom in the substrate. Thus, we hypothesized that if Cpd 0 is the preferred active oxidant, then the $\rm H_2O_2$ -initiated reactions would form noticeable amounts of epoxide-containing 6 when incubating TamI L295A with 1.

As anticipated, significant production of 6 was detected for reactions initiated with H₂O₂ and TamI L295A (Figure 6). Triple variant T252A T253A L295A also generates product 6 under these reaction conditions, albeit in diminished yields. Reactions with freshly prepared iodosobenzene led to the trace formation of 6, which further supported our hypothesis. To interrogate whether the ability to activate H2O2 as a cosubstrate for epoxidation is exclusive to biocatalyst TamI L295A, additional reactions with variant TamI L101A L295I and 1 were tested. Control reactions containing redox partners yielded the formation of 6 and 8 from 1, as previously observed (Figure 2),²¹ while no oxidation was observed with H₂O₂initiated reactions. This indicated that unlike TamI L295A, variant L101A L295I is not capable of using Cpd 0 for catalyzing epoxidation. Together with computational analysis and mutagenesis, these catalytic data suggest that TamI L295A has the flexibility to employ Cpd 0 as a viable oxidant for efficient alkene epoxidation of 1 to generate tirandamycin intermediate **6**.

2.2. Taml L295A-Catalyzed Unusual Iterative Oxidation Cascade Producing 9 and 10 from 7 or 7'. 2.2.1. Evidence for a Taml Reactive Peroxo-Iron Oxidant. To further probe the unusual oxidation cascade of Taml L295A, we hypothesized that the ferric hydroperoxo Cpd 0 form of the biocatalyst catalyzes epoxidation of $1 \rightarrow 6$, followed by Cpd I species catalyzing $6 \rightarrow 7$ or 7', and then shifts to a different oxidant species to open the epoxide of 7 or 7' to form 9 and 10. Inspired by the previous literature, ¹⁴ we hypothesized that the ferric-peroxo anion intermediate (species E) could perform a nucleophilic attack at C11 on intermediate 7 or 7'. This would open the epoxide while retaining stereochemistry at C12. Subsequent oxidation to the C11 ketone through radical or proton abstraction mechanisms

ACS Catalysis pubs.acs.org/acscatalysis Research Article

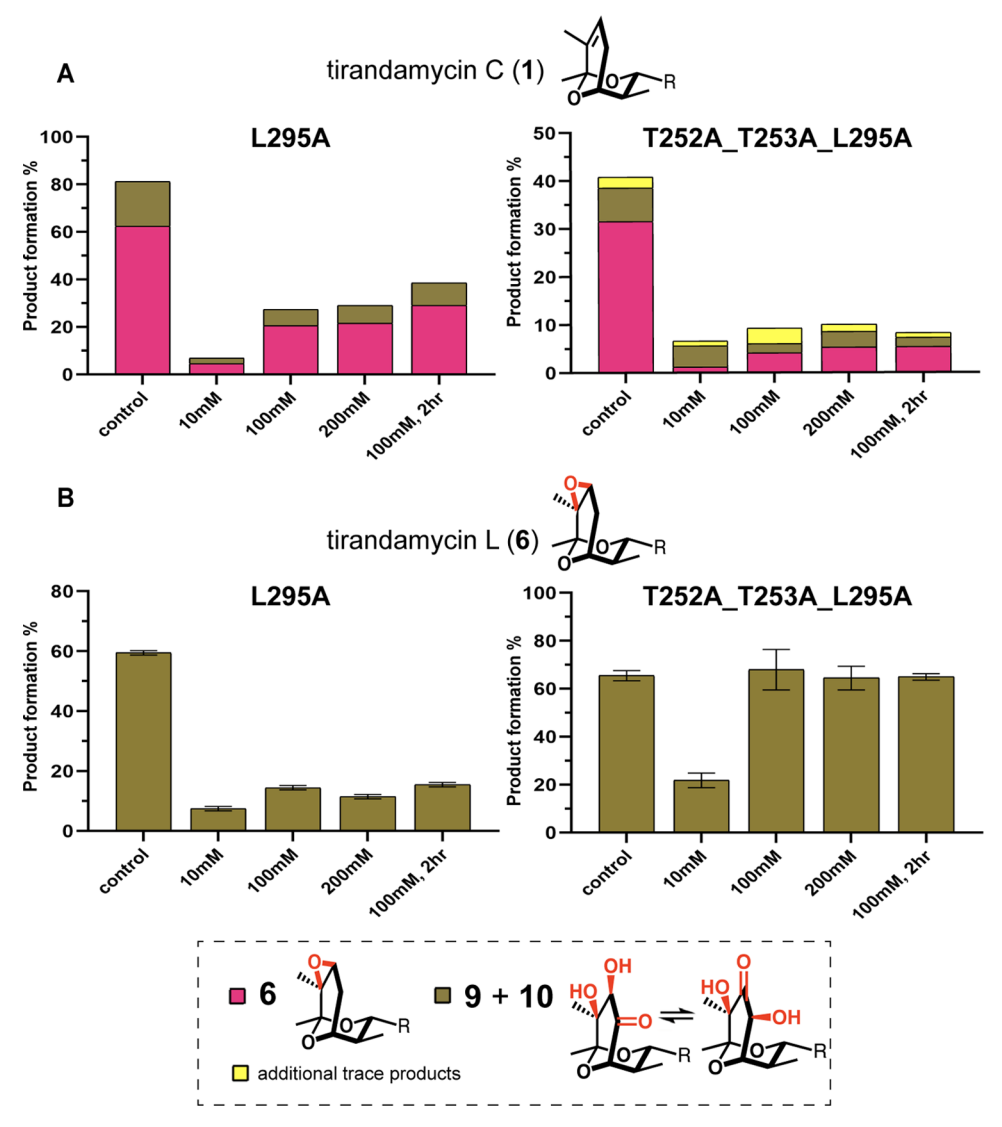


Figure 6. TamI-catalyzed oxidations via peroxide shunt pathway. Reactions were initiated with increasing concentrations of H_2O_2 and run for 30 min unless otherwise stated. The substrate is shown above bar graphs. The error bars represent the standard deviation of experiments performed in duplicate. For reactions initiated with iodosobenzene, see Supporting Information.

(Figure 3; blue box) would generate 10 and, via tautomerization, 9. To interrogate the plausibility of a peroxo anioncatalyzed oxidative cascade, we performed catalytic assays using 6 as the substrate. Previous work with P450cam, 25,26 P450cin, 13 CYP19A1, 27 P450-BM3, 28 and CYP17A1 29 suggests that mutating the conserved Glu251 acid residue disrupts the first proton transfer in the P450 catalytic cycle, favoring the formation of the nucleophilic peroxo-iron species (Figure 1; species E) and drastically reducing substrate oxidation activity. TamI variant E251Q L295A converts 6 to trioxidized 9 and 10, with yields comparable to L295A (Figure 5). The glutamic acid mutant displays a lower rate of hydrogen peroxide formation compared to L295A with 6, while no spin shift is observed with either enzyme. Adding ROS scavengers to the reaction of E251Q L295A and 6 led to a modest decrease in conversion compared to that of L295A. This could suggest that when using 6 and the glutamic acid variant as a biocatalyst, products 9 and 10 may result from shunt pathways. However, the response is not dose-dependent. Mutating the conserved acid residue to a neutral glutamine does not abolish catalytic activity. Instead, product formation is comparable to TamI

L295A. These data indicate that the glutamic acid residue is not critical for the oxidative cascade catalyzed by TamI L295A, suggesting that the peroxo-iron could compensate as a viable oxidant for the formation of **9** and **10** when Cpd I is compromised.

To address the identity of the iron-oxo species and variant mechanisms involved in the formation of multiple oxidized tirandamycin products, kinetic solvent isotope effect (KSIE) experiments were performed. Formation of Cpd I in the P450 catalytic cycle is dependent on the sequential transfer of two protons, a process that is typically attenuated when hydrogen has been replaced by deuterium. Hence, comparing the steadystate kinetic parameters of TamI-catalyzed reactions in H₂O versus D₂O-based buffers can be mechanistically informative. ¹⁷ Using saturating substrate concentrations, product formation and NADPH oxidation rates of P450 TamI were measured at pH/pD 7.4 (see Supporting Information for details). Deuterated samples were obtained by the exhaustive exchange of proteins in D₂O. The production of 2 from 1 occurred at a rate of 9.70 min⁻¹ for TamI WT in H₂O, while the rate lowered to 3.17 min⁻¹ in D₂O (Figure 7A). These values

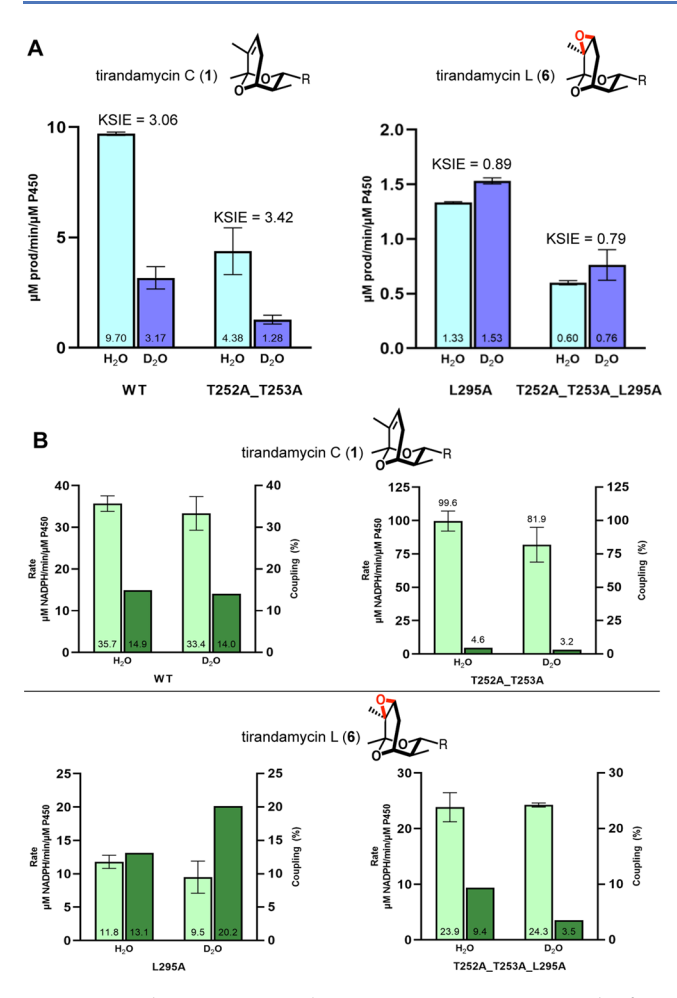


Figure 7. End-point assays with P450 TamI in $\rm H_2O$ vs $\rm D_2O$ buffers. Substrates are shown above each bar graph. The error bars represent the standard deviation of experiments performed in duplicate. (A) Steady-state kinetic solvent isotope effects (KSIE) observed for P450 TamI with tirandamycin C (1) and L (6). KSIE = $K_{\rm H}/K_{\rm D}$. The number inside the bar displays the value of catalytic activity. (B) Comparison of NADPH oxidation (light green) and coupling efficiency (dark green) by P450 TamI. The number inside the bar represents the corresponding calculated value. For exact values, refer to Table S2.

correspond to a significant KSIE of K_H/K_D = 3.06 for C10 hydroxylation, with similar values previously reported for other P450 systems catalyzing hydroxylation via Cpd I.¹⁷ When testing 6 with TamI L295A and triple variant T252A T253A L295A, the rate of product formation increased in the D2O-based buffer, resulting in a small inverse KSIE of 0.89 and 0.79, for the multistep cascade leading to 9 and 10 (Figure 7A). Although the potential influence of deuterium solvent on enzyme function is complex, these results implicate the role of peroxo-iron as a potential oxidant species catalyzing this cascade.³⁰ It is also important to consider that different pathways could be involved in the formation of Cpd I. For example, the rate-determining step for TamI WT could be the second and distal protonation of Cpd 0, while for TamI mutants, other events such as the O-O cleavage step could be rate-determining where using deuterated solvents could stabilize the peroxo-iron species. 11

TamI L295A shows an approximate 50% increase in coupling efficiency in D_2O compared to that in H_2O , with slightly lowered NADPH consumption values when using 6

(Figure 7B). On the other hand, triple mutant T252A_T253A_L295A displayed a twofold increase in NADPH consumption compared to L295A, with lowered coupling values. Together with KSIE data, a slight decrease in NADPH oxidation rates for the iterative oxidation of $6 \rightarrow 9$ and 10 with TamI L295A does not fully support a Cpd I-driven mechanism. Instead, these results suggest that inhibiting protonation of the peroxo-iron intermediate can promote productive oxidation rather than uncoupling to peroxide byproducts.

We sought to further investigate the potential involvement of a peroxo-iron species using computational methods.^a Thus, DFT calculations were conducted on a previously validated truncated model of the P450 TamI heme and tirandamycin bicyclic ketal.²¹ Oxidation of congeners 7 and 7' at the UB3LYP-D3(BJ)/def2-TZVPP/SMD(diethylether)// UB3LYP-D3(BJ)/def2-SVP/SMD(diethylether) level of theory and via peroxo-iron (species E) was explored. 14,31-35 Computations proceeding from 7' were found to be slightly lower in free energy (~1 kcal/mol) compared to those from 7 (Figure S16). Transition-state barriers for the addition of the peroxo-iron terminal oxygen into the epoxides of 7 and 7' were located for the doublet (²TS2) and quartet (⁴TS2) spin states and favor the doublet with a small preference for 7' (13.0 kcal/ mol) (Figure 8A). However, computational elaboration of this pathway proved challenging; while the endoperoxide intermediate (Int2) resulting from epoxide addition was successfully located for both 7 and 7' doublet states, we were unable to converge downstream product complexes or transition structures. While this convergence failure does not provide confirmation that peroxo-iron is a viable oxidant for the pathway, as is suggested by experimentation, it does not preclude peroxo-iron. Influence from the enzyme active site (e.g., hydrogen bonding from residues His102 and Thr299) may be required to activate Int2 for homolysis.

Moreover, we reasoned that our experimental results do not exclude the possibility of the superoxo-iron complex (Figure 1, species D) acting as an oxidant for an epoxide addition. Such a species is expected to persist in the TamI active site prior to an electron-transfer event involving ferredoxin. Openshell singlet, triplet, and quintet states were computed for the initial heme complex, of which the triplet pathway was lowest in energy. However, the addition of the triplet superoxo-iron species into the 7' epoxide exhibits a transition-state barrier of 24.3 kcal/mol relative to the starting material (Figure S18). As this barrier energy is significantly higher than those computed for the peroxo-iron pathway, we conclude that superoxo-iron is unlikely to be a viable oxidant species in this system.

2.2.2. Exploring Taml Cpd 0 Reactivity. Another pathway that we investigated was C11 C-H hydroxylation of 7' by Cpd 0 (species F) to form 9 and 10. A transition state could not be found for the initial C-H abstraction reaction. Given the favorable energetics for the Cpd I-facilitated hydrogen abstraction process and the activity of TamI in mutants exhibiting a disrupted proton transfer chain, we considered a pathway featuring C11-H-atom abstraction by a ferric-peroxo or ferric-superoxo species in both high-spin and low-spin configurations. A pathway featuring C11-H-atom abstraction from 7' to drive the incorporation of the distal oxygen of Cpd 0 and hydroxylation at C11 was explored. Ferric-peroxo and ferric-superoxo species in both high-spin and low-spin configurations were considered. In this pathway, the reaction of the substrate with either iron species involves a hydrogen

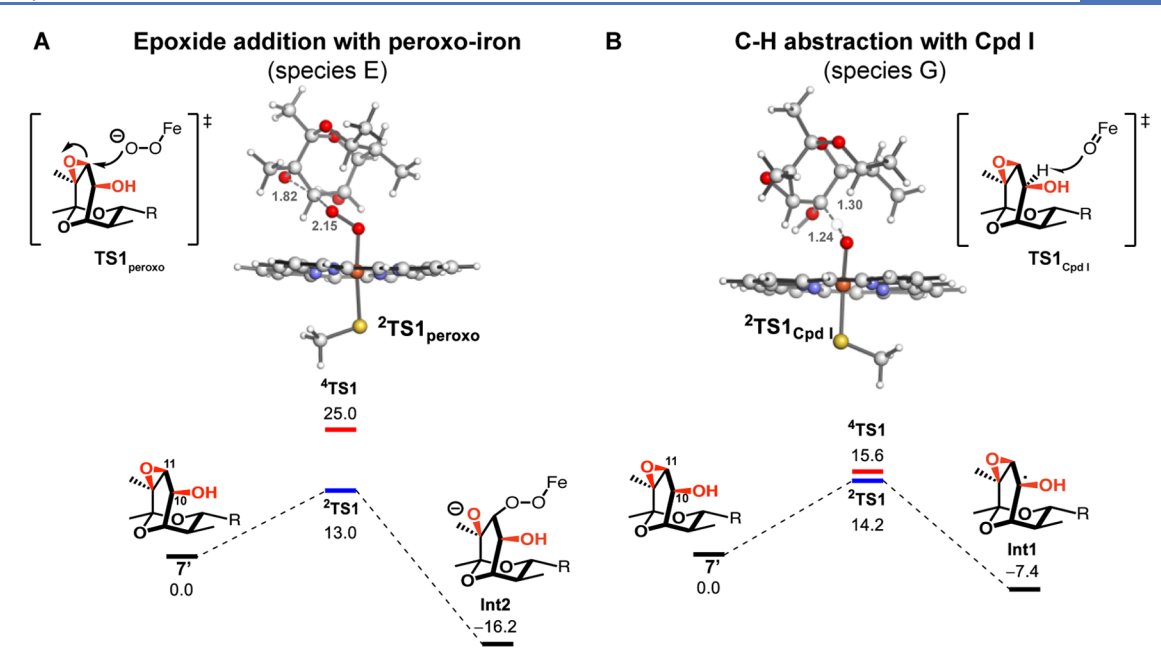


Figure 8. DFT calculations on P450 TamI and 7′ (epi-tirandamycin M). Gibbs free-energy values are shown in kcal/mol. The charge of the peroxo complex is −2. For additional calculations, see Supporting Information.

atom abstraction by the distal oxygen, generating a carbon-centered radical. This is followed by the concerted O—O bond homolysis and OH transfer to the radical. Subsequent deprotonation of the hydroxylated intermediate with epoxide ring opening ultimately leads to the formation of 9 and 10. The barriers for C—H abstraction are calculated to be 32.8 and 31.8 kcal/mol for the triplet and quintet ferric-superoxide species, respectively (Figure S19). Given the favorable energetics calculated for the nucleophilic peroxo-iron (species E), these computations show that hydrogen atom abstraction by either superoxo species is highly unlikely. An attempt was also made to identify either a high-spin or low-spin peroxo species that participates in the initial hydrogen atom abstraction, but no converged transition-state geometries were located.

End-point assays with substrate 6 and TamI variants L295A and T252A T253A L295A show comparable formation of 9 and 10 (Figure 5B). The threonine mutant shows relatively similar hydrogen peroxide formation rates compared to TamI L295A. No spin shift is observed with any of the TamI L295A variants bound to 6. When using H₂O₂ as a cosubstrate, reactions with T252A_T253A_L295A and 6 show product formation comparable to controls, while reactions with L295A and 6 display noticeable but decreased product formation. When initiating reactions with iodosobenzene and 6, no product is detected for any TamI variant. Adding ROS scavengers to the L295A-catalyzed reactions with 6 led to product formation comparable to controls for T252A L295A and L295A. A slight decrease was observed for T252A T253A L295A, indicating that the products in this reaction might result from shunt pathways, although a dosedependent pattern was not observed. Although these catalytic data do not conclusively discard Cpd 0 as a viable oxidant for catalyzing the production of 9 and 10, the significantly highenergy requirements calculated exclude Cpd 0-mediated catalysis.

2.2.3. Computational Investigations Support Cpd I Catalysis. Although the end-point assays described above shed light on the contribution of various oxidizing species in

L295A catalysis, they do not eliminate the possibility of a Cpd I-mediated mechanism. Thus, oxidative pathways via Cpd I species were explored computationally. Previous QM/MM investigations by Shaik et al. determine that the Cpd I and Cpd 0 have similar energies, which enables relative comparison of the energetics of the oxidant series.³⁸ First, the pathway for C-H abstraction of 7 with Cpd I was calculated. With 7 as the substrate, the TS barrier for C-H abstraction is calculated to be 15.3 kcal/mol for the doublet state and 16.1 kcal/mol for the quartet (Figure S20). The resulting product is 9.3 kcal/mol lower in energy than the starting material. This barrier exhibits a low energy similar to that calculated for peroxo anionfacilitated pathways (Figure 8A). The energy of the subsequent ring-opened product is -13.1 kcal/mol in ΔG , and the following H-atom abstraction from the resulting O radical to form Int3 has $\Delta G = -2.5$ kcal/mol (see Supporting Information for details). Hydroxyl group rebound from the Fe-OH species results in **Int4** ($\Delta G = -72.0 \text{ kcal/mol}$). Tautomerization affords 10 and 9 at -75.9 and -74.2 kcal/ mol, respectively. The analogous C-H abstraction was also calculated for 7' (Figure 8B). This substrate is 1.9 kcal/mol lower in energy than 7. The TS barrier for H-atom abstraction from 7' is 14.2 kcal/mol for the doublet (2TS1) and 15.6 kcal/ mol for the quartet (4TS1). These reasonable and low barriers and subsequent mechanism exergonicity suggest that pathways utilizing Cpd I as the oxidant are viable. While these data do not exclude the possibility of peroxo-iron as an oxidant, the low energy barrier and experimental support for the proposed Cpd I pathway provide compelling evidence that Cpd I is the preferred oxidant.

3. DISCUSSION

We have performed experimental and computational experiments to provide insights into the catalytically active species employed by P450 TamI L295A to catalyze epoxidation and the epoxide-opening oxidative cascade to form tirandamycin congeners. Specifically, we aimed to shed light on whether a single or multiple variant TamI P450 oxidizing species occur

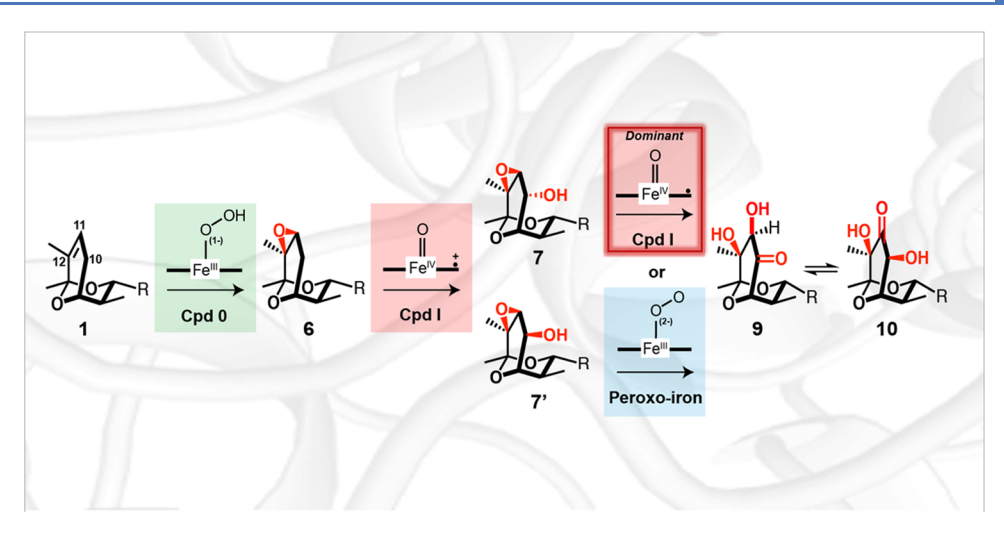


Figure 9. Oxidizing species involved in TamI L295A iterative oxidation catalysis. Cpd I (red box) is the dominant oxidant for the conversion of intermediate 7 or 7' to 9 and 10, although KSIE experiments indicated that the nucleophilic peroxo-iron (blue box) can be a viable alternate oxidant for this epoxide-opening cascade.

throughout the iterative cascade of $1 \rightarrow 6 \rightarrow 7$ or $7' \rightarrow 9$ and 10 (Figure 3). The experiments applied in this study suggest but do not conclusively determine the active oxidant.

To initiate our experimental approach, mutations were introduced in the highly conserved acid-alcohol pair of TamI (Glu251 and Thr252) to probe their role in oxygen activation and electron transfer (Figure 5). Earlier studies of bacterial P450s harboring a variation in the conserved alcohol residue displayed drastically diminished levels of hydroxylation activity and divergence to epoxidation reactivity, indicating the involvement of a Cpd 0 (species F) oxidant species.²² In L295A threonine variants, similar oxidation rates to L295A were obtained with substrate 1, without change in the chemoor regioselectivity patterns (Figure 5). These catalytic results could indicate that TamI L295A has the flexibility to exploit the use of heme-iron species other than Cpd I, including Cpd 0 for epoxidation of $1 \rightarrow 6$. A H_2O_2 -complexed species (the hydrogenated form of Cpd 0) was discarded based on the results obtained when adding ROS scavengers to the reactions of TamI L295A with 1. The presence of these scavengers was expected to capture most of the H₂O₂ present in the system.³⁹ Increased product formation was observed, indicating that the H₂O₂-shunt pathway to form 6 from 1 is not favorable. Mechanistic probes such as H₂O₂ and iodosobenzene were employed to further interrogate the involvement of different catalytically active species (Figure 6). TamI L295A was able to activate H_2O_2 for epoxidation of $1 \rightarrow 6$. Other TamI variants (including L295V, L101A L295I, and L244A L295V) catalyzing epoxidation or hydroxylation of 1 under normal conditions were not able to use H₂O₂ as a cosubstrate for oxidative reactivity. The results indicate that the Cpd 0 form of TamI L295A catalyzes the C11/12 diastereoselective epoxidation reaction of 1,40 an inference that was supported by computational analysis. Re-examination of published MD simulations of TamI L295A and 1 suggests that the C11/12 alkene is positioned at an angle disfavoring catalysis by Cpd I but that may be reached by the lengthened O-O bond in Cpd 0. This conclusion parallels P450 PimD's epoxidation reactivity via a presumed Cpd 0 iron species.⁵

Moreover, KSIE data demonstrated that the peroxo-iron species could be a viable oxidant for the conversion of $6 \rightarrow 7$ or $7' \rightarrow 9$ and 10 when H_2O in the reaction buffer is replaced

by D₂O, slowing down the formation of Cpd I (Figure 7). This was further validated by end-point assays with the E251Q_L295A mutant that is thought to interrupt the two proton transfers required for Cpd I, thus accumulating peroxoiron (Figure 1). DFT calculations for a peroxo-iron mechanism demonstrated low energy barriers for the initial TS and intermediate. Although downstream intermediates and products were not identified despite multiple efforts, computational experiments do not exclude peroxo-iron as a possible oxidant species. A Cpd I-mediated pathway toward the generation of 9 and 10 was also explored computationally. The low barriers and mechanism exergonicity obtained for a radical-induced ring opening of the epoxide in 7 and 7′ and subsequent oxygen rebound suggest that Cpd I is the preferred oxidant for TamI L295A's unique multistep oxidative pathway.

Experimental and computational methods have been recently combined to explore the active oxygen species in P450 biocatalysts catalyzing mechanistically distinct pathways on different substrates. As an example, P450-BM3 mutants performing sulfoxidation and hydroxylation on 1-thiochromanone and 1-tetralone substrates, respectively, were investigated.³⁹ Cpd I was found as the common oxidant species for both reaction processes. However, fewer efforts have been devoted to clarifying the mechanism of iterative oxidation at multiple carbon sites on a common substrate, in respect to the catalytically active oxygen species.

Elucidation of the catalytically active oxidant species in P450 TamI L295A facilitates the future engineering of enzymatic or chemical oxidation catalysts with iterative oxidation abilities. Favoring the formation of different iron oxygen species throughout a cascade reaction could enable mechanistically divergent oxidative pathways to be catalyzed on a common substrate. This could facilitate direct oxidative derivatization of multiple carbon atoms within complex molecules. For instance, a similar mutagenesis profile could be explored in the iterative bacterial P450 GfsF that harbors an active site Ala297 residue equivalent to the Leu295 site in TamI.41 The GfsF enzyme catalyzes a stepwise dual-cascade epoxidation followed by hydroxylation to form the macrolide antibiotic FD-891. The macrolide hydroxyl group is located β to the epoxide, parallel to the C10 hydroxyl in 7 and 7' that is β to the C11/12 epoxide. It is not unreasonable to imagine that engineering the

Ala297 residue may favor the formation of one catalytically active oxygen species over the other, facilitating epoxide opening to generate an α -ketone or a cis-diol-containing product, as observed in TamI L295A. A similar configuration for the positioning of the hydroxyl group relative to the epoxide within a substrate is found in the mycinamicin natural product. In this system, the iterative P450 MycG performs a strict hydroxylation followed by epoxidation, yielding a similar oxidation pattern to TamI L295A. Although the hydroxyl group is located at a tertiary carbon with no hydrogen atom available (unlike the case of GfsF or TamI systems), abstraction of the epoxy-hydrogen or nucleophilic opening of the epoxide could still occur to generate products similar to 9 and 10 if a different active oxidant species occurs.

The ability of TamI L295A to utilize H₂O₂ in lieu of molecular oxygen and NADPH for its iterative oxidation cascade is also noteworthy. This unexpected result represents a starting point for further design and engineering to improve the efficiency of peroxide-mediated TamI catalysis.²⁴ For example, adding small molecules to the reaction or introducing additional variations in the active site to stabilize H-bonding networks necessary for reactivity could facilitate an efficient peroxygenase activity for the enzyme,⁴⁰ maximizing its chemical utility.

Finally, elucidation of this pathway $(1 \rightarrow 6 \rightarrow 7 \text{ or } 7' \rightarrow 9)$ and 10) represents a unique oxidative outcome for P450 TamI and is particularly noteworthy (Figure 9). In the native system, substrate 1 is hydroxylated at C10 to form 2 prior to epoxidation at the C11/12 alkene in a strict sequence. TamI L295A and TamI L101A L295I represent the first two variants capable of deviating from the innate substrate reactivity to catalyze the most energetically demanding reaction first, a C11/12 epoxidation to produce 6 from 1. With epoxidecontaining 6, double variant L101A L295I catalyzes C18 methyl hydroxylation to form 8. In the present study, we demonstrated that TamI L295A is the only TamI biocatalyst able to invert the native order of oxidative steps and install a C10 hydroxyl on 6 to form 7 in vitro. This marks a distinct difference from the iterative P450 MycG that is not able to catalyze hydroxylation of a substrate that is initially epoxidized.⁴² The ability of TamI mutants to invert reactivity in a catalyst-controlled fashion facilitates core structure diversification to produce new analogues with unique patterns of oxidation.

4. CONCLUSIONS

The current work enables us to decipher the catalytic machinery that controls the mechanism of epoxidation and epoxide opening in the iterative cascade to produce trioxidized 9 and 10 from 1 by P450 TamI L295A. This work provides the first mechanistic picture for the catalytically active oxygen species involved in P450 TamI. The experimental results augmented by MD simulations and DFT calculations show that TamI L295A may include more than one active oxidant in its iterative cascade. Indeed, our data suggest that TamI L295A employs the ferric hydroperoxide Cpd 0 to catalyze the epoxidation of $1 \rightarrow 6$, then shifts to Cpd I for hydroxylation of $6 \rightarrow 7$ or 7', followed by Cpd I-mediated epoxide opening via a radical pathway to form C-H oxidation products 9 and 10 (Figure 9). Interestingly, our computational and kinetic data suggest that the nucleophilic peroxo-iron species serves as a viable oxidant for processing $6 \rightarrow 7$ or $7' \rightarrow 9$ and 10 when the formation of Cpd I is compromised. We expect that these

complementary approaches toward mechanistic investigations of iterative cytochrome P450 C–H functionalization and epoxidation biocatalysts will inspire further engineering efforts to generate novel, bioactive metabolites.

ASSOCIATED CONTENT

Supporting Information

The Supporting Information is available free of charge at https://pubs.acs.org/doi/10.1021/acscatal.2c00364.

Materials and methods; general; Streptomyces sp. 307-9 $\Delta tamI$ growth and extraction of tirandamycin C; large-scale enzymatic reactions and isolation of tirandamycin products; TamI production and purification; CO-bound reduced difference spectra of TamI; equilibrium substrate-binding assays; site-directed mutagenesis; enzymatic activity assays with TamI; measurement of hydrogen peroxide concentration in TamI reactions; the effect of reactive oxygen species scavengers on TamI reactions; determination of NADPH consumption rate, turnover frequency, and coupling efficiency; kinetic solvent isotope effects; and computational methods (PDF)

AUTHOR INFORMATION

Corresponding Author

David H. Sherman — Life Sciences Institute, Department of Medicinal Chemistry, Department of Chemistry, and Department of Microbiology and Immunology, University of Michigan, Ann Arbor, Michigan 48109, United States; orcid.org/0000-0001-8334-3647; Email: davidhs@umich.edu

Authors

Rosa V. Espinoza – Life Sciences Institute and Program in Chemical Biology, University of Michigan, Ann Arbor, Michigan 48109, United States

Mark A. Maskeri — Department of Chemistry and Biochemistry, University of California, Los Angeles, California 90095, United States; orcid.org/0000-0002-2630-8930

Aneta Turlik — Department of Chemistry and Biochemistry, University of California, Los Angeles, California 90095, United States; orcid.org/0000-0002-0907-8969

Anjanay Nangia – Department of Chemistry, Emory University, Atlanta, Georgia 30322, United States

Yogan Khatri – Life Sciences Institute, University of Michigan, Ann Arbor, Michigan 48109, United States; oocid.org/ 0000-0002-2432-7679

John Montgomery — Department of Chemistry and Department of Medicinal Chemistry, University of Michigan, Ann Arbor, Michigan 48109, United States; orcid.org/ 0000-0002-2229-0585

K. N. Houk – Department of Chemistry and Biochemistry, University of California, Los Angeles, California 90095, United States; orcid.org/0000-0002-8387-5261

Complete contact information is available at: https://pubs.acs.org/10.1021/acscatal.2c00364

Author Contributions

OM.A.M. and A.T. contributed equally.

Notes

The authors declare no competing financial interest.

ACKNOWLEDGMENTS

The authors thank the National Science Foundation under the CCI Center for Selective C–H Functionalization (CHE-1700982), the National Institutes of Health (R35 GM118101), and the Hans W. Vahlteich Professorship (to D.H.S.) for financial support. Calculations were performed on the Hoffman2 cluster at the University of California, Los Angeles, and the Extreme Science and Engineering Discovery Environment (XSEDE), supported by the National Science Foundation (Grant TG-CHE040013N).

ADDITIONAL NOTE

"As noted by a reviewer of this work, a consequence of invoking peroxo-iron for TamI L295A-catalyzed iterative oxidation of 6 to 9 and 10 is the initial oxidation of 1 to intermediates 6, 7, and 7' must, due to the proposed disrupted proton transfer mechanism, also proceed via peroxo-iron. We conducted preliminary DFT computations for this oxidation of 1 and located viable enthalpic barriers proceeding to 6. Please see Supporting Information Figure S17 for additional details.

REFERENCES

- (1) Denisov, I. G.; Makris, T. M.; Sligar, S. G.; Schlichting, I. Structure and chemistry of cytochrome P450. *Chem. Rev.* **2005**, *105*, 2253–2277.
- (2) Isin, E. M.; Guengerich, F. P. Complex reactions catalyzed by cytochrome P450 enzymes. *Biochim. Biophys. Acta* **2007**, 1770, 314–329.
- (3) Ortiz de Montellano, P. R. Cytochrome P450: Structure, Mechanism, and Biochemistry; Kluwer Academic/Plenum Publishers: New York, 2005; p 115.
- (4) Kumar, S. Engineering cytochrome P450 biocatalysts for biotechnology, medicine and bioremediation. *Expert Opin. Drug Metab. Toxicol.* **2010**, *6*, 115–131.
- (5) Bernhardt, R. Cytochromes P450 as versatile biocatalysts. *J. Biotechnol.* **2006**, 124, 128–145.
- (6) Ortiz de Montellano, P. R.; De Voss, J. J. Oxidizing species in the mechanism of cytochrome P450. *Nat. Prod. Rep.* **2002**, *19*, 477–493.
- (7) Shaik, S.; Kumar, D.; de Visser, S. P.; Altun, A.; Thiel, W. Theoretical perspective on the structure and mechanism of cytochrome P450 enzymes. *Chem. Rev.* **2005**, *105*, 2279–2328.
- (8) Meunier, B.; de Visser, S. P.; Shaik, S. Mechanism of oxidation reactions catalyzed by cytochrome P450 enzymes. *Chem. Rev.* **2004**, 104, 3947–3980.
- (9) Poulos, T. L. Heme enzyme structure and function. *Chem. Rev.* **2014**, *114*, 3919–3962.
- (10) Altarsha, M.; Benighaus, T.; Kumar, D.; Thiel, W. How is the reactivity of cytochrome P450cam affected by Thr252X mutation? A QM/MM study for X = serine, valine, alanine, glycine. *J. Am. Chem. Soc.* **2009**, *131*, 4755–4763.
- (11) Wang, B.; Li, C.; Dubey, K. D.; Shaik, S. Quantum mechanical/molecular mechanical calculated reactivity networks reveal how cytochrome P450cam and its T252A mutant select their oxidation pathways. J. Am. Chem. Soc. 2015, 137, 7379—7390.
- (12) Cupp-Vickery, J. R.; Han, O.; Hutchinson, C. R.; Poulos, T. L. Substrate-assisted catalysis in cytochrome P450eryF. *Nat. Struct. Biol.* **1996**, *3*, 632–637.
- (13) Stok, J. E.; Yamada, S.; Farlow, A. J.; Slessor, K. E.; De Voss, J. J. Cytochrome P450(cin) (CYP176A1) D241N: investigating the role of the conserved acid in the active site of cytochrome P450s. *Biochim. Biophys. Acta* **2013**, 1834, 688–696.
- (14) Gregory, M. C.; Denisov, I. G.; Grinkova, Y. V.; Khatri, Y.; Sligar, S. G. Kinetic solvent isotope effect in human P450 CYP17A1-mediated androgen formation: evidence for a reactive peroxoanion intermediate. *J. Am. Chem. Soc.* **2013**, *135*, 16245–16247.

- (15) Akhtar, M.; Njar, V. C.; Wright, J. N. Mechanistic studies on aromatase and related C-C bond cleaving P450 enzymes. *J. Steroid Biochem. Mol. Biol.* **1993**, 44, 375–387.
- (16) Kells, P. M.; Ouellet, H.; Santos-Aberturas, J.; Aparicio, J. F.; Podust, L. M. Structure of cytochrome P450 PimD suggests epoxidation of the polyene macrolide pimaricin occurs via a hydroperoxoferric intermediate. *Chem. Biol.* **2010**, *17*, 841–851.
- (17) Khatri, Y.; Luthra, A.; Duggal, R.; Sligar, S. G. Kinetic solvent isotope effect in steady-state turnover by CYP19A1 suggests involvement of Compound 1 for both hydroxylation and aromatization steps. *FEBS Lett.* **2014**, *588*, 3117–3122.
- (18) Ortiz de Montellano, P. R. Hydrocarbon hydroxylation by cytochrome P450 enzymes. *Chem. Rev.* **2010**, *110*, 932–948.
- (19) Ogliaro, F.; de Visser, S. P.; Cohen, S.; Sharma, P. K.; Shaik, S. Searching for the second oxidant in the catalytic cycle of cytochrome P450: a theoretical investigation of the iron(III)-hydroperoxo species and its epoxidation pathways. *J. Am. Chem. Soc.* **2002**, *124*, 2806–2817
- (20) Newmister, S. A.; Srivastava, K. R.; Espinoza, R. V.; Haatveit, K. C.; Khatri, Y.; Martini, R. M.; Garcia-Borras, M.; Podust, L. M.; Houk, K. N.; Sherman, D. H. Molecular basis of iterative C-H oxidation by TamI, a multifunctional P450 monooxygenase from the tirandamycin biosynthetic pathway. *ACS Catal.* **2020**, *10*, 13445–13454.
- (21) Espinoza, R. V.; Haatveit, K. C.; Grossman, S. W.; Tan, J. Y.; McGlade, C. A.; Khatri, Y.; Newmister, S. A.; Schmidt, J. J.; Garcia-Borràs, M.; Montgomery, J.; Houk, K. N.; Sherman, D. H. Engineering P450 TamI as an iterative biocatalyst for selective latestage C–H functionalization and epoxidation of tirandamycin antibiotics. *ACS Catal.* **2021**, *11*, 8304–8316.
- (22) Jin, S.; Makris, T. M.; Bryson, T. A.; Sligar, S. G.; Dawson, J. H. Epoxidation of olefins by hydroperoxo-ferric cytochrome P450. *J. Am. Chem. Soc.* **2003**, *125*, 3406–3407.
- (23) Coleman, T.; Stok, J. E.; Podgorski, M. N.; Bruning, J. B.; De Voss, J. J.; Bell, S. G. Structural insights into the role of the acidalcohol pair of residues required for dioxygen activation in cytochrome P450 enzymes. *J. Biol. Inorg. Chem.* 2020, 25, 583–596.
- (24) Joo, H.; Lin, Z.; Arnold, F. H. Laboratory evolution of peroxide-mediated cytochrome P450 hydroxylation. *Nature* **1999**, 399, 670–673.
- (25) Altarsha, M.; Wang, D.; Benighaus, T.; Kumar, D.; Thiel, W. QM/MM study of the second proton transfer in the catalytic cycle of the D251N mutant of cytochrome P450cam. *J. Phys. Chem. B* **2009**, 113, 9577–9588.
- (26) Vidakovic, M.; Sligar, S. G.; Li, H.; Poulos, T. L. Understanding the role of the essential Asp251 in cytochrome P450cam using site-directed mutagenesis, crystallography, and kinetic solvent isotope effect. *Biochemistry* **1998**, *37*, 9211–9219.
- (27) Lo, J.; Di Nardo, G.; Griswold, J.; Egbuta, C.; Jiang, W.; Gilardi, G.; Ghosh, D. Structural basis for the functional roles of critical residues in human cytochrome p450 aromatase. *Biochemistry* **2013**, 52, 5821–5829.
- (28) Yeom, H.; Sligar, S. G. Oxygen activation by cytochrome P450BM-3: effects of mutating an active site acidic residue. *Arch. Biochem. Biophys.* **1997**, 337, 209–216.
- (29) Peng, H. M.; Im, S. C.; Pearl, N. M.; Turcu, A. F.; Rege, J.; Waskell, L.; Auchus, R. J. Cytochrome b_5 activates the 17,20-lyase activity of human cytochrome P450 17A1 by increasing the coupling of NADPH consumption to androgen production. *Biochemistry* **2016**, 55, 4356–4365.
- (30) Yoshimoto, F. K.; Gonzalez, E.; Auchus, R. J.; Guengerich, F. P. Mechanism of 17α ,20-lyase and new hydroxylation reactions of human cytochrome P450 17A1: ¹⁸O labeling and oxygen surrogate evidence for a role of a perferryl oxygen. *J. Biol. Chem.* **2016**, 291, 17143–17164.
- (31) Becke, A. D. Density-functional thermochemistry. III. The role of exact exchange. *J. Chem. Phys.* **1993**, *98*, 5648–5652.
- (32) Grimme, S.; Ehrlich, S.; Goerigk, L. Effect of the damping function in dispersion corrected density functional theory. *J. Comput. Chem.* **2011**, 32, 1456–1465.

- (33) Lee, C.; Y, W.; Parr, R. G. Development of the Colle-Salvetti correlation-energy formula into a functional of the electron density. *Phys. Rev. B* **1988**, *37*, 785–789.
- (34) Stephens, P. J.; Devlin, F. J.; Chabalowski, C. F.; Frisch, M. J. Ab initio calculation of vibrational absorption and circular dichroism spectra using density functional force fields. *J. Phys. Chem. A* **1994**, 98, 11623–11627.
- (35) Weigend, F.; Ahlrichs, R. Balanced basis sets of split valence, triple zeta valence and quadruple zeta valence quality for H to Rn: design and assessment of accuracy. *Phys. Chem. Chem. Phys.* **2005**, *7*, 3297–3305.
- (36) Chung, L. W.; Li, X.; Sugimoto, H.; Shiro, Y.; Morokuma, K. ONIOM study on a missing piece in our understanding of heme chemistry: bacterial tryptophan 2,3-dioxygenase with dual oxidants. *J. Am. Chem. Soc.* **2010**, *132*, 11993–12005.
- (37) Chung, L. W.; Li, X.; Hirao, H.; Morokuma, K. Comparative reactivity of ferric-superoxo and ferryl-oxo species in heme and nonheme complexes. *J. Am. Chem. Soc.* **2011**, *133*, 20076–20079.
- (38) Zheng, J.; Wang, D.; Thiel, W.; Shaik, S. QM/MM study of mechanisms for compound I formation in the catalytic cycle of cytochrome P450cam. *J. Am. Chem. Soc.* **2006**, *128*, 13204–13215.
- (39) Wang, J. B.; Huang, Q.; Peng, W.; Wu, P.; Yu, D.; Chen, B.; Wang, B.; Reetz, M. T. P450-BM3-catalyzed sulfoxidation versus hydroxylation: a common or two different catalytically active species? *J. Am. Chem. Soc.* **2020**, *142*, 2068–2073.
- (40) Zhang, X.; Jiang, Y.; Chen, Q.; Dong, S.; Feng, Y.; Cong, Z.; Shaik, S.; Wang, B. H-Bonding networks dictate the molecular mechanism of $\rm H_2O_2$ activation by P450. *ACS Catal.* **2021**, *11*, 8774–8785.
- (41) Miyanaga, A.; Takayanagi, R.; Furuya, T.; Kawamata, A.; Itagaki, T.; Iwabuchi, Y.; Kanoh, N.; Kudo, F.; Eguchi, T. Substrate recognition by a dual-function P450 monooxygenase GfsF involved in FD-891 biosynthesis. *ChemBioChem* **2017**, *18*, 2179–2187.
- (42) Yang, S.; DeMars, M. D., IInd; Grandner, J. M.; Olson, N. M.; Anzai, Y.; Sherman, D. H.; Houk, K. N. Computational-based mechanistic study and engineering of cytochrome P450 MycG for selective oxidation of 16-membered macrolide antibiotics. *J. Am. Chem. Soc.* **2020**, *142*, 17981–17988.

